Phase asymmetry ultrasound despeckling with fractional anisotropic diffusion and total variation

Article *in* IEEE Transactions on Image Processing · November 2019

DOI: 10.1109/TIP.2019.2953361

Phase asymmetry ultrasound despeckling with fractional anisotropic diffusion and total variation

Kunqiang Mei, Bin Hu, Baowei Fei, and Binjie Qin*, *Member, IEEE*

***Abstract*—We propose an ultrasound speckle filtering method for not only preserving various edge features but also filtering tissue-dependent complex speckle noises in ultrasound images. The key idea is to detect these various edges using a phase congruence-based edge significance measure called phase asymmetry (PAS), which is invariant to the intensity amplitude of edges and takes 0 in non-edge smooth regions and 1 at the idea step edge, while also taking intermediate values at slowly varying ramp edges. By leveraging the PAS metric in designing weighting coefficients to maintain a balance between fractional-order anisotropic diffusion and total variation (TV) filters in TV cost function, we propose a new fractional TV framework to not only achieve the best despeckling performance with ramp edge preservation but also reduce the staircase effect produced by integral-order filters. Then, we exploit the PAS metric in designing a new fractional-order diffusion coefficient to properly preserve low-contrast edges in diffusion filtering. Finally, different from fixed fractional-order diffusion filters, an adaptive fractional order is introduced based on the PAS metric to enhance various weak edges in the spatially transitional areas between objects. The proposed fractional TV model is minimized using the gradient descent method to obtain the final denoised image. The experimental results and real application of ultrasound breast image segmentation show that the proposed method outperforms other state-of-the-art ultrasound despeckling filters for both speckle reduction and feature preservation in terms of visual evaluation and quantitative indices. The best scores on feature similarity indices have achieved 0.867, 0.844 and 0.834 under three different levels of noise, while the best breast ultrasound segmentation accuracy in terms of the mean and median dice similarity coefficient are 96.25% and 96.15%, respectively.**

***Index Terms*—ultrasound despeckling, speckle noise, fractional-order diffusion filter, fractional-order TV filter, edge detection, phase congruency, phase asymmetry, image denoising.**

I. Introduction

CURRENT advanced image denoising [1][2] and image enhancement algorithms [3][4] are developed to solve the difficult and urgent open problems of feature preservation in the removal of complex signal-dependent noises for challenging real applications. In these recent research developments, feature-preserving ultrasound despeckling [5][6] is most desired in clinical applications due to the ubiquity of the ultrasound imaging modality given its noninvasiveness, low cost and convenience; however, its quality is relatively poor compared with other medical imaging modalities. The main reason for quality degradation in ultrasound images is the presence of an inherent imaging artefact called speckle, which results from constructive and destructive coherent interferences of backscattered echoes from the scatterers [5][6][7]. Speckle is commonly interpreted as a locally correlated noise that reduces image contrast and conceals fine feature details [8], causing negative effects on medical diagnosis and reduction of the accuracy of subsequent image processing such as segmentation and registration [7]. Furthermore, extracting coherent feature patterns from the noisy ultrasound signals is necessary for super-resolution ultrasound microvessel imaging [9] and 3D reconstruction from a series of 2D freehand ultrasound images [10]. Therefore, it is very important to remove speckle noise with satisfactory feature preservation for accurate diagnosis and analysis in many applications.

However, feature-preserving speckle reduction is a challenging task, since speckle noise is known to be tissue-dependent and it manifests itself in the form of multiplicative noise, which means that the intensity of speckle can change sharply and the intensity of variance of speckle is comparable to or even larger than that of the features[11]. Therefore, simply employing intensity-based gradient information cannot accurately distinguish edges from speckle noise, especially for low-contrast edges. Failing to preserve various edges will damage other features of structures (or shapes) whose boundaries are composed of the edges. Existing edge-preserving image processing techniques [13][14] are likely to damage some low-contrast features, since they regard some low-contrast edges as speckle noise and remove these edges after noise removal by exploring intensity-based gradient information.

Various speckle reduction filters are proposed to solve the abovementioned challenges, including local adaptive filters, non-local means (NLM) filters and diffusion filters. The local adaptive filters such as Frost [14] filters and bilateral filters [15] rectify a pixel by averaging its neighbouring pixels. In their experimental comparison, Chen *et al.* [16] indicated that the bilateral filtering is not as good as the other methods such as diffusion filters for the edge preservation in ultrasound images. Moreover, the squeeze box filter (SBF) [17] rectifies only local extrema at each iteration by replacing them with the local mean. However, these local adaptive filters are sensitive to the shape and size of local windows. The NLM algorithms

Manuscript received April 14, 2018; accepted October 27, 2018; This work was supported by the National Natural Science Foundation of China (61271320), Medical Engineering Cross Fund of Shanghai Jiao Tong University (YG2014MS29), and Translational Medicine Cross Fund of Shanghai Jiao Tong University (ZH2018ZDA19).

Kunqiang Mei and Binjie Qin are with the School of Biomedical Engineering, Shanghai Jiao Tong University, Shanghai, 200240, China. E-mail: bjqin@sjtu.edu.cn.

Bin Hu is with Department of Ultrasound in Medicine, Shanghai Jiao Tong University Affiliated Sixth People's Hospital, Shanghai Institute of Ultrasound in Medicine, Shanghai, 200233, China.

Baowei Fei is with Department of Bioengineering, Erik Jonsson School of Engineering and Computer Science, University of Texas at Dallas, Richardson, TX 75080, USA.

assume that natural images contain many similar features. NLM algorithms group similar features from different image patches and remove noise by a weighted average of similar features. Coupe *et al.* [18] proposed the optimal Bayesian NLM (OBNLM) filter to process ultrasound images in non-Gaussian speckle noise circumstances. An improved OBNLM filter is proposed by Zhou *et al.* [19] to iteratively refine the filtering model by deducing the key probability density function according to the statistical characteristic of the speckle noise. Recently, Zhu *et al.* [20] developed a non-local low-rank framework (NLLRF) for ultrasound speckle reduction, which leverages a guidance image to improve the performance of patch selection. However, NLM algorithms usually mix different features into the same patch cluster in the case of a large number of features, causing some important details to become indiscernible after noise removal [21].

In regard to diffusion filtering, after Perona and Malik proposed the well-known anisotropic diffusion (AD) filter [22], both the speckle reducing anisotropic diffusion (SRAD) [23] filter and the detail preserving anisotropic diffusion (DPAD) [24] filter have been modified based on the AD filter. The SRAD filter added a parameter related to the noise estimate into the diffusion coefficient, while the DPAD filter adopted an improved noise estimator to improve the despeckling performance. The oriented speckle reducing anisotropic diffusion [25] filter modified the diffusion coefficient with the local directional variance of the image intensity. Using an edge indicator to distinguish between sharp and ramp edges in images, Chen *et al.* [16] proposed to adaptively determine the diffusion coefficient for introducing isotropic diffusion in flat and ramp regions and anisotropic diffusion in sharp edges for medical images. Using the information about image gradient and grey levels of the image, a doubly degenerate diffusion model [26] with robust speckle reduction performance [27] is proposed to remove multiplicative noise. However, all of these diffusion filters employ the local intensity-based gradient or grey level information to identify edges, failing to detect and preserve low-contrast edges. Moreover, the gradient difference between sharp edges and ramp edges is not obvious, and therefore anisotropic diffusions based on the image gradient are prone to cause the staircase effect in the regions of ramp edges. To reduce the staircase effect, Bai and Feng [28] proposed a fixed fractional-order AD (FAD) model for image denoising. Nevertheless, the fixed fractional-order diffusion filter neglects the differences among various image regions. Recently, Flores *et al.* [8] developed an anisotropic diffusion filter guided by the log-Gabor filters (ADLG) instead of the intensity-based gradient. However, ADLG fails to achieve satisfactory feature preservation. Based on nonlinear AD for filtering noisy coefficients in the transform domain, some wavelet [29] and shearlet-based [30] transform-domain filtering approaches are combined with AD to exploit the advantages of multi-resolution analysis, noise removal and edge preservation. However, these methods have a high computational cost due to the transformation and anti-transformation steps and may insert or manipulate artificial frequencies in the recovered image.

Essentially, edge detection and image denoising depend on each other, leading to a "chicken-or-the-egg" causality dilemma in ultrasound despeckling. The abovementioned diffusion filters that fail to accurately identify edges from speckle noises cannot achieve satisfactory feature preservation after speckle filtering. As an important image feature, the edge is a basic element of other features, such as ridges, valleys, textures and boundaries of structures, such that failing to preserve the edges will render these structure features inviable [31]. Therefore, robustly detecting the edge from the noisy image is half the battle of ultrasound despeckling. To solve the drawback of local methods [32] that use local intensity information for edge detection, Ofir *et al.* [33] consider the edge detection as a search approach in a large set of feasible curves by hierarchically constructing difference filters that match the curves traced by the sought edges. However, this method has a high computational cost on large and noisy images containing long edges and has a great limitation in searching weak irregular texture boundaries [2] in noisy images. Cogranne *et al.* [34] implement edge detection as a regression problem with a regression surface based on local image content model. Such an idea of transferring image processing into searching a regression's coefficients from the context information of a neighbourhood area is successfully and widely used in image denoising [35], image reconstruction [36], image registration [37][38], and so on. However the computation of the regression's coefficients for indicating the edges' presence is still sensitive to the sharp change of local intensity information in the presence of multiplicative noise.

To solve the drawback of intensity-based edge detectors, some local phase-based edge detection methods [39][40] were developed in ultrasound imaging. In analytically representing images using spatially varying sinusoidal waves, the local phase informs us about the location and orientation of image features, while the amplitude provides only information on their intensity. More specifically, local phase is an illumination and contrast-invariant measure of feature significance based on a model of feature perception called the local-energy model developed by Morrone *et al.* [41][42]. This model postulates that features are perceived at points in an image, where the Fourier components are maximally in phase. A wide range of feature types give rise to points of high-phase congruency. These include step edges, line and roof edges, and Mach bands. The first local phase-based work for successfully detecting the boundary in echocardiographic images is from Mulet-Parada and Noble [43]. We then use the method introduced in [44] to construct a phase congruency (PC)-based feature indicator called phase symmetry (PS) and phase asymmetry (PAS, all acronyms in this paper are listed in Table I) depending on the image feature type to be detected. Both PS and PAS are special patterns of PC [44]. Specifically, PS can be used to detect symmetry features for image enhancement such as bone surface enhancement [45] and vessel enhancement [4], while PAS can be used to identify edge features for ultrasound image denoising [39] and segmentation [40]. Zhu *et al.* [39] employ the phase congruency-based PAS metric to extract edge features on the phase domain for efficiently and robustly distinguishing features and speckle noise during the ultrasound despeckling process. Inspired by these works, we use the PAS to detect various types of edge features. In ultrasound images,

TABLE I
ACRONYMS.

Acronym	Definition
PAS	Phase asymmetry
PS	Phase symmetry
PC	Phase congruency
AD	Anisotropic diffusion
FAD	Fractional-order anisotropic diffusion
TV	Total variation
FTV	Fractional-order TV
NLM	Non-local means
SBF	Squeeze box filter
OBNLM	Optimal Bayesian NLM
SRAD	Speckle reducing anisotropic diffusion
DPAD	Detail preserving anisotropic diffusion
ADLG	AD filter guided by the log-Gabor filter
PFDTV	Phase asymmetry fractional AD and TV
G-L	Grünwald–Letnikov
PSNR	Peak signal-to-noise ratio
FSIM	Feature similarity index
MSSIM	Mean structural similarity index
BUS	Breast ultrasound
DSC	Dice similarity coefficient
JS	Jaccard similarity
HD	Hausdorff distance
HM	Hausdorff mean

almost all of the real edges are weak ramp edges of various slopes rather than ideal step edges. Particularly, low-contrast edges refer to the weak ramp edges with low-step amplitude. In regard to the symmetry features in images, they are also made of edges. If we preserve their edges using the PAS indicator, the symmetry features will be preserved properly.

The PAS metric provides a good measure of asymmetric image features and can effectively detect various edges from backgrounds of images[39][40][45]. Specifically, the PAS metric represents the edge significance [42][44] of each point and varies from 0 to 1, taking 0 (no-edge significance) in ideal smooth regions and taking 1 (a highly significant edge point) at sharp step edges. Generally, points at the same edge have a similar edge significance. As the steepness of a ramp edge reduces, the PAS values of the edge points also reduce. Thus, we can distinguish different ramp edges based on the PAS values of edge points. To overcome the deficiencies of the abovementioned algorithms and achieve a better despeckling performance both quantitatively and visually, we propose a Phase asymmetry Fractional anisotropic Diffusion and Total Variation (PFDTV) method to preserve various edges and remove speckle noises in ultrasound images.

The contributions of our method are four-fold. Firstly, to the best of our knowledge, this is the first fractional TV framework that leverages the PAS metric in designing weighting coefficients to maintain a balance between FAD and FTV filters in achieving not only the best despeckling performance with ramp edge preservation but also in reducing the staircase effect produced by integral-order filters. Secondly, a new diffusion coefficient of the FAD filter is proposed to properly preserve low-contrast edges by exploiting the edge identification of the PAS metric instead of intensity-based gradient information in traditional AD filters. Thirdly, our framework adjusts the fractional order adaptively based on the PAS metrics to enhance various edges: on the one hand, different from the fixed fractional-order diffusion filters [46][47] that neglect the differences between smooth regions and the various edges in the spatially transitional border regions, our adaptive strategy adopts high-fractional order for the various edges and uses low-fractional order for smooth regions; on the other hand, our framework assigns an adaptive fractional order to each edge point according to the edge significance of the PAS metric for each edge point to obtain a better edge enhancement. Finaly, the proposed despeckling method is applied to remove complex cancer-dependent noises for ease of accurate breast cancer delineation in real ultrasound image segmentation.

The remainder of this article is organized as follows. The theoretical backgrounds about phase asymmetry, fractional-order differential and fractional-order AD and TV filters are introduced in Section II. The details of the PFDTV method are introduced in Section III. The experimental results are reported in Section IV. Some research issues and future directions with a brief conclusion are summarized in Section V.

II. THEORETICAL BACKGROUNDS

A. Phase Asymmetry

For the characteristics of ultrasound images, solely employing gradient information to identify edges cannot achieve satisfactory feature preservation. This work detects edges by adopting the phase-based PAS measure, which can efficiently separate edges from smooth regions. According to a human perception study [44], at the points of perceivable step edges, the absolute values of even symmetric filter responses are small while the absolute values of odd symmetric filter responses are large. In other words, the difference between the odd and the even filter responses is large. According to this finding, PAS [48] provides a good measure of the asymmetric image feature for detecting step and ramp-like edges.

To calculate the PAS metric of a 2D signal f, we first need to extract its local phase and local amplitude with a 2D signal decomposition method. In the past decades, there has been an increasing interest in decomposing multidimensional signals using spatially varying sinusoidal waves. As the understanding of the theory advanced, amplitude- and frequency-modulation (AM–FM) decompositions [49][50][51] have been applied in a large range of problems, for example, ultrasound image texture analysis [52], ultrasound image segmentation [40] and medical imaging [53]. The monogenic signal [54] was proposed to decompose the 2D signal f into the local phase and local amplitude based on Riesz filters. The monogenic signal f_M is defined as: $f_M = (f, f_R) = (f, r_1 * f, r_2 * f)$, where f_R is the

Riesz transform of f, $r_1(x_1, x_2)$ and $r_2(x_1, x_2)$ are the spatial representation of Riesz filters, shown as follows:

$$\begin{aligned} r_1(x_1, x_2) &= \frac{-x_1}{2\pi\left(x_1^2+x_2^2\right)^{3/2}} \\ r_2(x_1, x_2) &= \frac{-x_2}{2\pi\left(x_1^2+x_2^2\right)^{3/2}} \end{aligned} \tag{1}$$

Since natural images generally contain a wide range of frequencies, the monogenic signal f_M needs to be combined with a set of bandpass quadrature filters b. The monogenic signal f_M becomes $f_M = (b * f, b * r_1 * f, b * r_2 * f) = (e_s, o_s)$, where e_s and o_s denote the scalar-valued even and vector-valued odd filter responses respectively.

Several families of bandpass filters b have been proposed to calculate the e_s and o_s; we adopt a Cauchy kernel as the bandpass filter, since the Cauchy kernel has an analytical expression in the spatial and the Fourier domain [55]. In the frequency domain, the 2D isotropic Cauchy kernel is defined by the following:

$$C(w) = n_c \left|w\right|^a \exp\left(-s\left|w\right|\right), a \geq 1 \tag{2}$$

where $w = (w_1, w_2)$ is the angular frequency, s is the scaling parameter, $n_c = \left(\frac{\pi\, 4^{a+1}\, s^{2a+1}}{\Gamma(2a+1)}\right)^{\frac{1}{2}}$, $\Gamma(\cdot)$ is the gamma function, and a is the bandwidth. We set $a = 1.58$, as suggested in [39].

To identify different edges accurately, Kovesi [44] suggested to use the PAS measure over a number of scales. Therefore, we define the multiple-scale PAS as follows:

$$PA = \sum_s \frac{\lfloor |o_s| - |e_s| - T_s \rfloor}{\sqrt{e_s^2 + o_s^2} + \varepsilon} \tag{3}$$

where PA is the PAS metric, ε is a small positive constant to avoid division by zero, T_s is the scale-specific noise threshold, $\lfloor \cdot \rfloor$ represents zeroing of negative values, and s is the scaling parameter of Cauchy kernels. Specifically, s plays an important role in obtaining an accurate edge map, since increasing s will regularize the continuity (or connect the breakpoints) in the boundaries but slightly lose details somewhat in edge detection.

Fig. 1 shows an example of the PAS measure at different scales. We can find that the discontinuities in some boundaries in the PAS maps at $s = 5$ and $s = 10$ will reduce the accuracy of locating edges. The boundaries in the PAS maps at $s = 20$ and $s = 25$ have good continuity, but some details are lost. The PAS map at $s = 15$ maintains a balance between the boundary continuity and detail preservation. Thus, we choose $s = 15$ to detect edges in real ultrasound images.

PAS provides an absolute measure of the edge significance of points. The PAS metric varies from 0 to 1, taking 0 (indicating non-edge significance) in ideal smooth regions and taking 1 (indicating high edge significance) at sharp step edges. In general, points at the same edge have a similar edge significance. As the steepness of a step edge reduces, the PAS values of the edge points also reduce. Due to PAS being invariant to brightness or contrast, low-contrast edges can be detected efficiently. For the real ramp edges in ultrasound images, the PAS values of these edge points are less than 1.

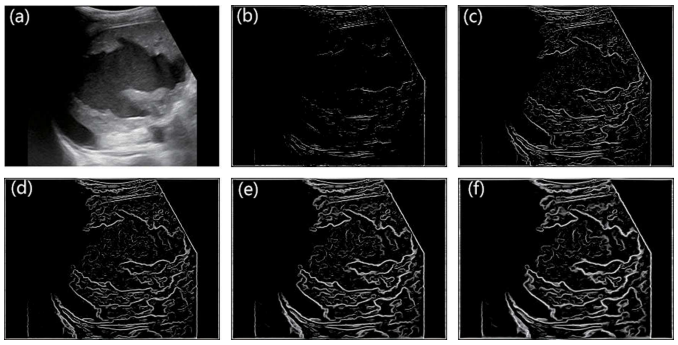

Fig. 1. Example of PAS measure at different scales. (a) The ultrasound image of the spleen; the PAS map of: (b) $s = 5$, (c) $s = 10$, (d) $s = 15$, (e) $s = 20$, (f) $s = 25$.

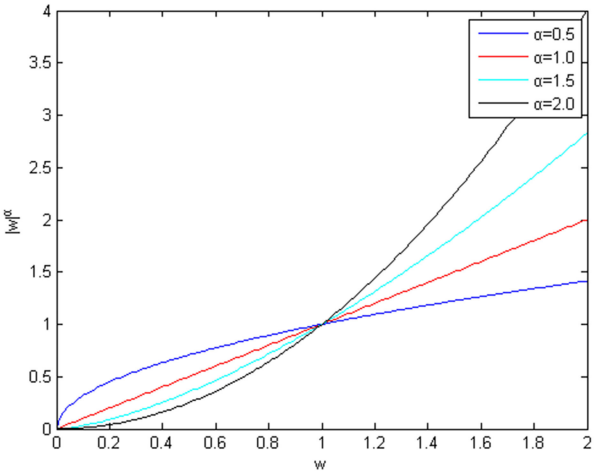

Fig. 2. The curves of the amplitude-frequency characteristic of the fractional differential with different orders.

B. Fractional-order differential

The fractional-order differential performs better in enhancing edges than integer-order differential during image processing [47]. For a square differentiable signal $f(x) \in L^2(R)$, its fractional-order differential is given as follows:

$$D^\alpha f(x) = \frac{d^\alpha f(x)}{d\, x^\alpha} \tag{4}$$

where α is a positive real number. The Fourier transform of $D^\alpha f(x)$ is as follows:

$$\begin{aligned} D^\alpha f(x) \overset{FT}{\Leftrightarrow} (\hat{D}^\alpha f)(w) &= (iw)^\alpha \hat{f}(w) \\ &= |w|^\alpha \exp\left[i\, \theta^\alpha(w)\right] \hat{f}(w) \\ &= |w|^\alpha \exp\left[\frac{\alpha\pi i}{2}\mathrm{sgn}(w)\right] \hat{f}(w) \end{aligned} \tag{5}$$

where w is the angular frequency, $\mathrm{sgn}(\cdot)$ denotes the numeric symbol of the integer part, and $(iw)^\alpha = |w|^\alpha \exp\left[\frac{\alpha\pi i}{2}\mathrm{sgn}(w)\right]$ is the filter function of the fractional differential filter. According to the filter function, we can draw the curves of the amplitude-frequency characteristic of the fractional differential with different α, as depicted in Fig. 2. From Fig. 2, it is obviously seen that in the low-frequency field with $0 < w < 1$, the fractional differential acts as an

attenuation function. Nevertheless, in the section with $w > 1$, the fractional differential enlarges the amplitude values, and the enhanced amplitude will be stronger as the fractional order α increases. Taking into account the amplitude enhancement in the high-frequency field, we effectively apply the fractional-order differential into edge enhancement in image denoising.

Diffusion filters tend to reduce the edge contrast during smoothing. Although traditional fractional-order diffusion filters usually adopt one fixed fractional order to process the image, this strategy neglects the differences between smooth regions and the various edges in spatially transitional border regions [47]. Edges will be weakened if a low-fractional order is used, while smooth regions will be ignored if a high-fractional order is adopted. This drawback will inevitably cause some details to be damaged after noise removal [46]. Therefore, a more reasonable choice is to assign the fractional-order α adaptively based on the PAS metric as in Sec. III-A for enhancing various edges in ultrasound images.

Currently, there are three commonly used definitions of fractional calculus: the Capotu definition, the Grünwald–Letnikov (G-L) definition and the Riemann–Liouville (R-L) [56][57]. Since the G-L definition expresses a function using the weighted sum around the function, the G-L definition is suitable for signal processing. According to [58], the α-order differential of signal $f(x)$ is defined by the G-L as follows:

$$D^{\alpha} f(x) \triangleq \lim_{h \to 0} \frac{1}{h^{\alpha}} \sum_{k=0}^{[\frac{d-c}{h}]} (-1)^{l} \binom{\alpha}{l} f(x - lh) \tag{6}$$

where α is the fractional order, $[c, d]$ is the duration of $f(x)$, the integer part of $\frac{d-c}{h}$ is $[\frac{d-c}{h}]$, and the formula $\binom{\alpha}{l}$ is the binomial coefficient defined as follows:

$$\binom{\alpha}{l} = \frac{\Gamma(\alpha + 1)}{\Gamma(l+1)\Gamma(\alpha - l + 1)} \tag{7}$$

where $\Gamma(n) = (n-1)!$ is the gamma function.

C. Fractional-order AD filter and fractional-order TV filter

The following partial differential equation defines the original AD [22] filter:

$$\frac{\partial u}{\partial t} = div\left[c\left(|\nabla u|\right) \cdot \nabla u\right], \tag{8}$$

where div is the divergence operator, $|\nabla u|$ is the absolute value of ∇u, and $c(\cdot)$ is the diffusion coefficient related to the magnitude of local image gradient ∇u. A possible diffusion coefficient function [22] is defined as follows:

$$c\left(|\nabla u|\right) = 1/\left[1 + |\nabla u|^2 / k^2\right] \tag{9}$$

where k is the gradient threshold. To preserve edges, this diffusion coefficient will reduce the diffusivity at edges that have a large magnitude of the local intensity-based gradient.

The TV method for image processing is to search numerical approximation to the lowest cost function of image, the variational principle is the foundation of this method [59]. Variational model for speckle noise removal [60] normally consists of regularized term and data fidelity term. The classical TV filter [59] is proposed as follows:

$$E(u) = \int_{\Omega} \left(|\nabla u| + \frac{\lambda}{2} |u - u_0|^2 \right) \tag{10}$$

where $|\nabla u|$ denotes the total variation, $|u - u_0|^2$ is the fidelity term, λ is the regularization parameter and u_0 is the noisy image.

To reduce the staircase effect caused by classical AD and TV filters, the variational FAD [28] and FTV [61] filters were developed. The variational FAD filter [28] is shown as follows:

$$E\left(\mathrm{u}\right) = \int_{\Omega} f\left(|\nabla^{\alpha} u|\right) d\Omega \tag{11}$$

where α is the fractional order, $\nabla^{\alpha} u = \left(\nabla_x^{\alpha} u, \nabla_y^{\alpha} u\right)$, $|\nabla^{\alpha} u| = \sqrt{\left(\nabla_x^{\alpha} u\right)^2 + \left(\nabla_y^{\alpha} u\right)^2}$, and $f\left(|\nabla^{\alpha} u|\right) \geq 0$ is an increasing function associated with the diffusion coefficient in the AD [22] filter, shown as follows:

$$c\left(t\right) = \frac{f'\left(\sqrt{t}\right)}{\sqrt{t}} \tag{12}$$

Zhang and Wei [61] proposed the following FTV filter:

$$E\left(u\right) = \int_{\Omega} \left(|\nabla^{\alpha} u| + \frac{\lambda}{2} |u - u_0|^2 \right) dxdy \tag{13}$$

where α is the fractional order, $|\nabla^{\alpha} u|$ denotes the total variation, $|u - u_0|^2$ is the fidelity term, λ is the regularization parameter and u_0 is the noisy image.

III. OVERALL OF PFDTV

A. The proposed model

The PFDTV method proposes a new TV framework with phase asymmetry to guide adaptive fractional-order total variation and diffusion filter for feature-preserving ultrasound despeckling. Specifically, the proposed TV cost function combining equation (11) and (13) balances the FAD filter and FTV filter for achieving the best performance of preserving ramp edges, and the TV cost function is defined as follows:

$$E\left(u\right) = \int_{\Omega} \left[\varphi f\left(|\nabla^{\alpha} u|\right) + \gamma |\nabla^{\alpha} u| + \frac{\lambda}{2} |u - u_0|^2 \right] dxdy \tag{14}$$

where α is the adaptive fractional order, φ and γ are the weighted coefficients that control the relative importance of the FAD and FTV filters, and λ is the regularization parameter. The speckle filtering result is closely related to λ: the greater the value of λ is, the more noisy the filtered image achieves; the smaller the value of λ is, the more blurry the edge feature becomes. Two types of regularization parameter selection methods have been introduced in terms of locally-adaptive and global performance measures. In this paper, the parameter λ is chosen so that the best global PSNR of despeckled image is obtained [61]. We empirically set λ as 0.01 after synthetic image despeckling experiments. Regarding

the weighted coefficients, we design them based on the PAS metric shown as follows:

$$\begin{cases} \varphi = (PA-1)^2 \\ \gamma = PA(2-PA) \end{cases} \tag{15}$$

where PA is the PA metric that is updated in each iteration for accurately obtaining the edge significance of each point.

Based on the above strategy, when PA is close to 0, we emphasize the role of the FAD filter in smoothing regions. When PA is close to 1, we highlight the role of the FTV filter in the boundary regions for edge preservation. Because the PA values of edge points for real ramp edges are less than 1, the FAD filter also plays a key role in processing these weak edges in the spatially transitional border regions.

However, the FAD filter solely integrates intensity-based gradient into the diffusion coefficient, causing some low-contrast edges to be removed after noise removal. To overcome this drawback, we integrate the PAS metric into the diffusion coefficient. The PAS measure can efficiently identify low-contrast edges due to its invariance to brightness or contrast. Furthermore, the PAS metric value is only related to the edge significance of each point. We alter the function $f\left(|\nabla^{\alpha} u|\right)$ by modifying its diffusion coefficient $c(\cdot)$ according to (12). The modified diffusion coefficient is shown as follows:

$$c\left(|\nabla^{\alpha} u|, PA\right) = 1/\left[1+\frac{|\nabla^{\alpha} u|\cdot(1+254\cdot PA)}{k_1^2}\right] \tag{16}$$

where $k_1 = k_0\, e^{-0.05(n_{iter}-1)}$ is the modified version of k in (9). Here, n_{iter} is the number of iterations, and k_0 is a positive constant that is related to the noise level.

Given that diffusion filters reduce the edge contrast during smoothing, it is essential to design a proper strategy to enhance various edges in an ultrasound image. According to the discussion in Sec. II-B, we can set the fractional-order α as a monotone increasing function of the PAS value of the ultrasound images to adaptively enhance the various edges in the ultrasound images. Specifically, we adopt a logarithmic function to describe the adaptive adjustment of the order of fractional derivative by modifying the adaptive fractional-order strategy in [46] as follows:

$$\alpha = 1+\log_2\left(1+PA^2\right) \tag{17}$$

where PA is the PAS metric. This functional setting ensures that $\alpha \in (1,2)$. The adaptive strategy of the PFDTV method assigns low-fractional order to preserve smooth regions and uses high-fractional order to enhance the various edges in spatially transitional border regions.

In fact, the PAS metric shows the edge significance of each point. As the PAS value increases, the edge significance of the point also increases and the point is more likely to be an edge point. According to (17), a larger PAS metric yields a larger α that can produce better edge enhancement. The PFDTV method will adopt relatively high-fractional order to enhance the most significant edge points compared with the least significant edge points, so that we can properly preserve various edges and obtain a better image enhancement.

B. Numerical Solver

We leverage the Euler-Lagrange equation [62] to solve the cost function (14). Assuming the solution u of this cost function $E(u)$ is known, then this solution must make $E(u)$ minimum. In other words, adding any slight perturbation to u will make the cost function larger. When the perturbation goes to 0, the derivative of the cost function with respect to the perturbation is 0. The perturbation is represented as a very small continuous function $\eta \in C^{\infty}(\Omega)$ multiplied by a perturbation factor e. Define the following:

$$\begin{aligned} &\Phi(e) := E(u+e\eta) \\ &= \int_{\Omega}\left[\varphi f\left(|\nabla^{\alpha}(u+e\eta)|\right)+\gamma\,|\nabla^{\alpha}(u+e\eta)|\right]dxdy \\ &+\int_{\Omega}\left(\tfrac{\lambda}{2}\,|u+e\eta-u_0|^2\right)dxdy \end{aligned} \tag{18}$$

We first take the derivative of $\Phi(e)$ and obtain the following:

$$\begin{aligned} &\Phi'(e) = \tfrac{d}{de}\Phi(e) = \\ &\varphi\int_{\Omega}\left(f'\left(|\nabla^{\alpha}(u+e\eta)|\right)\frac{\nabla_x^{\alpha}(u+e\eta)\,\nabla_x^{\alpha}\eta+\nabla_y^{\alpha}(u+e\eta)\,\nabla_y^{\alpha}\eta}{\sqrt{(\nabla_x^{\alpha}(u+e\eta))^2+\left(\nabla_y^{\alpha}(u+e\eta)\right)^2}}\right)dxdy \\ &+\gamma\int_{\Omega}\left(\frac{\nabla_x^{\alpha}(u+e\eta)\,\nabla_x^{\alpha}\eta+\nabla_y^{\alpha}(u+e\eta)\,\nabla_y^{\alpha}\eta}{\sqrt{(\nabla_x^{\alpha}(u+e\eta))^2+\left(\nabla_y^{\alpha}(u+e\eta)\right)^2}}\right)dxdy \\ &+\lambda\int_{\Omega}(u+e\eta-u_0)\eta dxdy, \end{aligned} \tag{19}$$

Let $e=0$, and we have the following:

$$\begin{aligned} &\Phi'(0) = \\ &\varphi\int_{\Omega}\left(c\left(|\nabla^{\alpha}u|^2, PA^2\right)\left(\nabla_x^{\alpha}u\,\nabla_x^{\alpha}\eta+\nabla_y^{\alpha}u\,\nabla_y^{\alpha}\eta\right)\right)dxdy \\ &+\gamma\int_{\Omega}\frac{\nabla_x^{\alpha}u\,\nabla_x^{\alpha}\eta+\nabla_y^{\alpha}u\,\nabla_y^{\alpha}\eta}{|\nabla^{\alpha}u|}dxdy \\ &+\lambda\int_{\Omega}(u-u_0)\eta dxdy \end{aligned} \tag{20}$$

where $|\nabla^{\alpha}u| = \sqrt{\left(\nabla_x^{\alpha}u\right)^2+\left(\nabla_y^{\alpha}u\right)^2}$. According to the previous analysis for finding the solution u, we can obtain $\Phi'(0)=0$. To simplify (20), we use the definition of the adjoint operator to simplify the following term:

$$\nabla_x^{\alpha}u\,\nabla_x^{\alpha}\eta+\nabla_y^{\alpha}u\,\nabla_y^{\alpha}\eta = \left(\left(\nabla_x^{\alpha}\right)^*\nabla_x^{\alpha}u+\left(\nabla_y^{\alpha}\right)^*\nabla_y^{\alpha}u\right)\eta \tag{21}$$

where $\left(\nabla_x^{\alpha}\right)^*$ and $\left(\nabla_y^{\alpha}\right)^*$ are the adjoint operators of ∇_x^{α} and ∇_y^{α} respectively [63]. Based on the above analysis, we obtain the simplified form of (20) as follows:

$$\begin{aligned} &\Phi'(0) = \\ &\varphi\int_{\Omega}c\left(|\nabla^{\alpha}u|^2, PA^2\right)\left(\left(\nabla_x^{\alpha}\right)^*\nabla_x^{\alpha}u+\left(\nabla_y^{\alpha}\right)^*\nabla_y^{\alpha}u\right)\eta\mathrm{d}x dy \\ &+\gamma\int_{\Omega}\frac{\left(\nabla_x^{\alpha}\right)^*\nabla_x^{\alpha}u+\left(\nabla_y^{\alpha}\right)^*\nabla_y^{\alpha}u}{|\nabla^{\alpha}u|}\eta\mathrm{d}x dy \\ &+\lambda\int_{\Omega}(u-u_0)\,\eta\mathrm{d}x dy \end{aligned} \tag{22}$$

For all $\eta \in C^{\infty}(\Omega)$, the Euler-Lagrange equation is:

$$\begin{aligned} &\varphi c\left(|\nabla^{\alpha}u|^2, PA^2\right)\left(\left(\nabla_x^{\alpha}\right)^*\nabla_x^{\alpha}u+\left(\nabla_y^{\alpha}\right)^*\nabla_y^{\alpha}u\right) \\ &+\gamma\frac{\left(\nabla_x^{\alpha}\right)^*\nabla_x^{\alpha}u+\left(\nabla_y^{\alpha}\right)^*\nabla_y^{\alpha}u}{|\nabla^{\alpha}u|}+\lambda(u-u_0) = 0 \end{aligned} \tag{23}$$

where u is the solution that minimizes the cost function.

Let ∇E denote the first derivative of the cost function $E(u)$; a necessary condition for u to be the extreme point of $E(u)$ is that $\nabla E = 0$. Thus, ∇E holds that:

$$\begin{aligned}\nabla E = \varphi c(|\nabla^\alpha u|^2, PA^2)((\nabla_x^\alpha)^* \nabla_x^\alpha u + (\nabla_y^\alpha)^* \nabla_y^\alpha u) \\ +\gamma \frac{(\nabla_x^\alpha)^* \nabla_x^\alpha u + (\nabla_y^\alpha)^* \nabla_y^\alpha u}{|\nabla^\alpha u|} + \lambda(u - u_0)\end{aligned} \tag{24}$$

The desired u is computed via gradient descent method as in [64]. Specifically, we introduce an artificial time parameter Δt and take a small step in the direction of $-\nabla E$, *i.e.*, $u^{n+1} = u^n + \Delta t(-\nabla E)$. Finally, we will obtain the desired image u that minimizes the cost function $E(u)$.

C. Numerical algorithm

To compute (24) numerically, we use the G-L fractional differential to facilitate the numerical implementation. We assume that the size of a given image u is $X \times Y$, where X and Y are the numbers of pixels in the vertical and horizontal direction respectively. Then, we can obtain the discretized schemes of $\nabla_{\mathrm{x}}^\alpha$, ∇_y^α , $(\nabla_x^\alpha)^*$ and $\left(\nabla_y^\alpha\right)^*$, shown as follows:

$$\begin{cases} \nabla_x^\alpha u_{i.j} = \sum_{l=0}^{j} (-1)^l \binom{\alpha}{l} u_{i,j-l} \\ \nabla_y^\alpha u_{i.j} = \sum_{l=0}^{i} (-1)^l \binom{\alpha}{l} u_{i-l,j} \end{cases} \tag{25}$$

$$\begin{cases} (\nabla_x^\alpha)^* u_{i.j} = \sum_{l=0}^{Y-1-j} (-1)^k \binom{\alpha}{l} u_{i,j+l} \\ \left(\nabla_y^\alpha\right)^* u_{i.j} = \sum_{l=0}^{X-1-i} (-1)^k \binom{\alpha}{l} u_{i+l,j} \end{cases} \tag{26}$$

where $i = 0, 1, ..., X-1, j = 0, 1, ..., Y-1$, and the formula $\binom{\alpha}{l}$ is the binomial coefficient defined as $\binom{\alpha}{l} = \frac{\Gamma(\alpha+1)}{\Gamma(l+1)\Gamma(\alpha-l+1)}$, where Γ is the gamma function. Let the following:

$$\begin{cases} FAD_{\mathrm{x}} u_{i,j} = \sum_{l=0}^{Y-1-j} (-1)^l \binom{\alpha}{l} \frac{k_1^2 \nabla_x^\alpha u_{i,j+l}}{k_1^2 + |\nabla^\alpha u_{i,j+l}|^2 [1 + 254 PA(u_{i,j+l})]^2} \\ FAD_y u_{i,j} = \sum_{l=0}^{X-1-i} (-1)^l \binom{\alpha}{l} \frac{k_1^2 \nabla_y^\alpha u_{i+l,j}}{k_1^2 + |\nabla^\alpha u_{i+l,j}|^2 [1 + 254 PA(\mathrm{u}_{i+l,j})]^2} \end{cases} \tag{27}$$

$$\begin{cases} FTV_x u_{i,j} = \sum_{l=0}^{Y-1-j} (-1)^l \binom{\alpha}{l} \frac{\nabla_x^\alpha u_{i,j+l}}{\sqrt{(\nabla_x^\alpha u_{i,j+l})^2 + \left(\nabla_y^\alpha u_{i,j+l}\right)^2 + \varepsilon}} \\ FTV_y u_{i,j} = \sum_{l=0}^{X-1-i} (-1)^l \binom{\alpha}{l} \frac{\nabla_y^\alpha u_{i+l,j}}{\sqrt{(\nabla_x^\alpha u_{i+l,j})^2 + \left(\nabla_y^\alpha u_{i+l,j}\right)^2 + \varepsilon}} \end{cases} \tag{28}$$

where $PA(u_{i,j})$ is the PAS value of pixel $u_{i,j}$, and ε is very small positive number. We summarize the optimization process in Algorithm 1.

Algorithm 1 Feature-preserving speckle reduction.

Input: noisy ultrasound image u_0, the values of s, k_0, time step Δt and iteration number n_{iter}

Output: the despeckled image u

1: Initialize $u^{(0)} = u_0, \varepsilon = 0.0001, n = 1$,
2: **for all** $n < n_{iter}$ **do**
3: Compute $FAD_x\, u_{i,j}^{(n)}, FAD_y\, u_{i,j}^{(n)}, FTV_x\, u_{i,j}^{(n)}$ and $FTV_y\, u_{i,j}^{(n)}$ using (27) and (28)
4: Compute $u^{(n+1)}$ through the following procedure: $u_{i,j}^{(n+1)} = u_{i,j}^{(n)} - \Delta t[\varphi(FAD_x\, u_{i,j}^{(n)} + FAD_y\, u_{i,j}^{(n)}) + \gamma(FTV_x\, u_{i,j}^{(n)} + FTV_y\, u_{i,j}^{(n)}) + \lambda(u_{i,j}^{(n)} - u_{i,j}^{(0)})]$
5: Set $n = n + 1$
6: **end for**
7: Set the despeckled image $u = u^{(n)}$
8: **return** u

IV. EXPERIMENTAL RESULTS

Experiments with synthetic and clinical ultrasound images were carried out to show the performance of the proposed PFDTV method[1]. Several well-known ultrasound despeckling filters were used for comparison, including Frost [14], SRAD [23], OBNLM [18], SBF [17], ADLG [8], and NLLRF [20]. We directly requested the source code of the SBF filter from its authors. In regard to other filters, we obtained the source codes from the cited authors' websites listed in their works.

A. Synthetic image experiment

For the purpose of quantitative comparisons, we generated noise over the ground truth image by employing the synthetic speckle noise model that is widely used in the literature [18][20][39]. The noise model is given by the following:

$$u(x_i) = v(x_i) + v(x_i)\tau(x_i), \tau(x_i) \sim N(0, \sigma^2) \tag{29}$$

where $v(x_i)$ and $u(x_i)$ are the pixel intensities of pixel x_i in the noise-free image and the synthesized noisy image respectively, and $\tau(x_i)$ is a zero-mean Gaussian noise with variance σ^2. We applied this noise model to Fig. 3(a), which consists of smooth regions and various local features. Three levels of noise were tested by setting $\sigma^2 = \{0.2; 0.4; 0.6\}$. Fig. 3(b) depicts the synthetic image with noise variance $\sigma^2 = 0.2$. To quantitatively evaluate the performance of each filter, the peak signal-to-noise ratio (PSNR) [65][66], mean structural similarity (MSSIM) [67] and feature similarity index (FSIM) [68] were adopted in this paper. Specifically, FSIM[2] is designed for measuring the ability of preserving features, and it takes values between 0 and 1, and 1 denotes the best performance of feature preservation.

To fairly compare the overall performance of each filter in noise reduction and feature preservation, each filter needs to achieve the best performance by setting its optimal parameters. The optimal parameters need to be selected based on a quantitative metric so that the PSNR metric is accepted as a gold standard as in [2][69]. This is because PSNR regards

[1]The source code is available at http://www.escience.cn/people/bjqin/research.html
[2]http://sse.tongji.edu.cn/linzhang/IQA/FSIM/FSIM.htm

TABLE II
COMPARISON OF THE PSNR, MSSIM AND FSIM VALUES AMONG DIFFERENT FILTERS.

	PSNR			MSSIM			FSIM		
	0.2	0.4	0.6	0.2	0.4	0.6	0.2	0.4	0.6
Frost	25.773	23.840	22.955	0.721	0.638	0.576	0.848	0.818	0.797
SRAD	26.760	25.272	24.282	0.743	0.697	0.679	0.816	0.777	0.764
OBNLM	26.496	24.974	24.121	0.742	0.696	0.679	0.822	0.794	0.764
SBF	22.502	22.303	22.214	0.695	0.648	0.657	0.825	0.807	0.790
ADLG	24.585	22.945	22.360	0.676	0.625	0.599	0.786	0.758	0.745
NLLRF	27.409	25.536	24.282	0.763	0.711	0.699	0.825	0.798	0.768
PFDTV	**27.721**	**25.994**	**25.103**	**0.783**	**0.732**	**0.713**	**0.867**	**0.844**	**0.834**

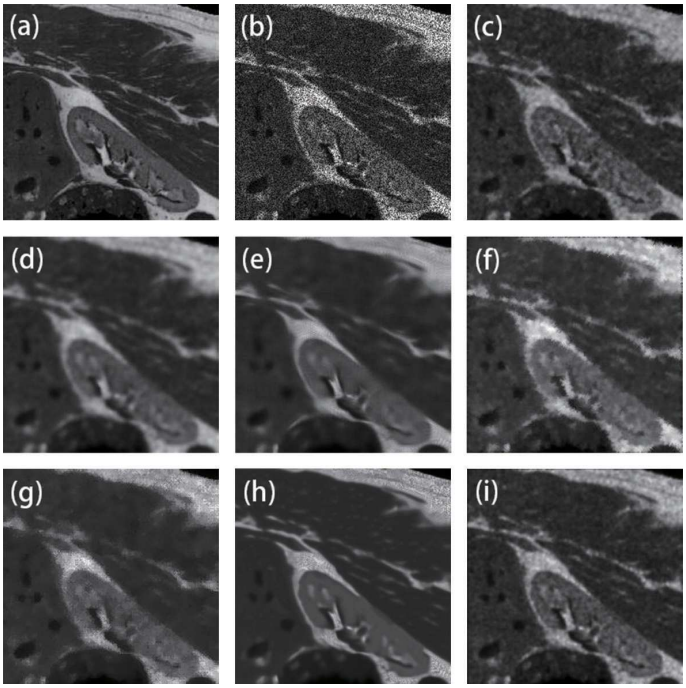

Fig. 3. Results of different filters for the synthetic image. (a) Original image, (b) original image corrupted with speckle noise with variance $\sigma^2 = 0.2$, despeckled result by (c) Frost ($W = 5 \times 5$) , (d) SRAD ($\Delta t = 0.3, n_{iter} = 60$), (e) OBNLM ($M = 5, \alpha = 6, h = 3$) , (f) SBF ($W$=$3 \times 3, \mathrm{n_{iter}} = 9$), (g) ADLG ($\Delta \mathrm{t} = 0.3, n_{iter} = 50$), (h) NLLRF ($\beta = 20, H = 10$), and (i) **PFDTV** ($\Delta t = 0.3, s = 20, k_0 = 100, n_{iter} = 7$).

the structural information and the nonstructural information as the same in terms of the contribution towards the performance, whereas SSIM and FSIM put more emphasis on the structural information [2]. Therefore, we obtain the optimal parameters of each filter when achieving the highest value of the PSNR metric. PFDTV has the following parameters: s is the scale of the Cauchy kernel, Δt is the time step, n_{iter} is the iteration number, and k_0 is for the noise level.

Fig. 3 depicts the denoised images of different filters with their optimal parameters. The Frost filter has clear features, but it retains a significant level of noise. The SRAD remove noise better but produces smoother edges and removes some low-contrast features compared with Frost. Though OBNLM and NLLRF have good performance in high-contrast features, they cause some meaningful low-contrast features to become indiscernible after noise removal. Both SBF and ADLG produce fuzzy boundaries, and ADLG removes considerable details. Therefore, the PFDTV method achieves the best performances in noise removal and feature preservation.

Table II compares the PSNR, MSSIM and FSIM values for different filters. The proposed PFDTV method achieves the highest PNSR, MSSIM and FSIM. The highest PSNR denotes that the despeckled image of our method produces a lower image distortion compared with other filters. The highest MSSIM represents that the despeckled image of our method is most similar to the original image. The highest FSIM represents that the PFDTV method outperforms other filters in feature preservation.

B. Clinical image experiment

Since real ultrasound images are all affected by speckle noise, there are no ground truth image and gold standard for quantitative performance evaluation on real ultrasound images. Therefore, we employed different types of clinical ultrasound images to visually verify the performance of the PFDTV method. The clinical ultrasound images were all downloaded from the public dataset.[3]

The real ultrasound image experiment has no ground truth image and gold standard to find the optimal parameters in terms of quantifiable performance criteria. Thus, we adjust the parameters of the PFDTV method to obtain the best visual effect. The visual performance of our method is closely associated with three parameters: s, k_0 and n_{iter}. According to the analysis in Section II-A, we set the scale s of the PAS measure as 15. k_0 is a positive constant that is related to the the noise level, and n_{iter} is the number of iterations.

The parameter k_0 is an important parameter that is related to the noise level estimation. Noise level estimation is a prerequisite for various detail-preserving image denoising methods [21] but has remained as an unsolved challenging problem in ultrasound image despeckling. According to (16), if k_0 is set to a large value, a large diffusion coefficient is obtained that will cause some details to be damaged after speckle reduction. However, if k_0 is set to a small value, a small diffusion coefficient is achieved that will increase

[3]http://www.ultrasoundcases.info

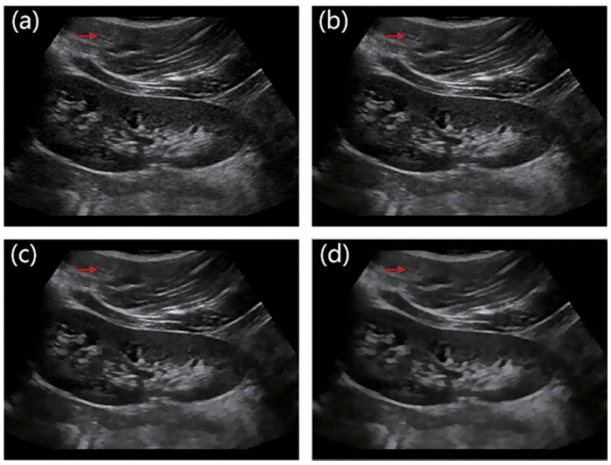

Fig. 4. Example of the despeckled image of different k_0. (a) The original ultrasound image; the despeckled result of (b) $k_0 = 5$, (c) $k_0 = 20$, (d) $k_0 = 100$.

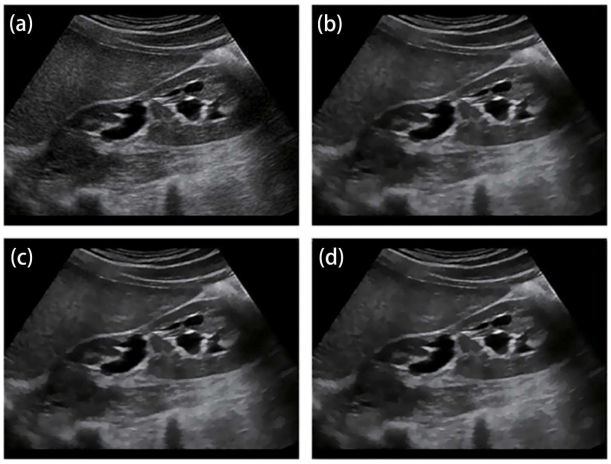

Fig. 5. Example of the despeckled images of different n_{iter}. (a) The original ultrasound image; the despeckled result of (b) $n_{iter} = 8$, (c) $n_{iter} = 25$, and (d) $n_{iter} = 50$.

computational costs in the despeckling process. To explore the impact of parameter k_0, we set k_0 with different values. Fig. 4 depicts the despeckled results of different k_0. It is observed that there is a significant level of noise in the despeckled result of $k_0 = 5$. As indicated by the red arrow in Fig. 4(d), the meaningful detail is damaged after noise removal in the case of $k_0 = 100$. Our method achieves not only satisfactory feature preservation but also desirable noise reduction in the case of $k_0 = 20$. In real image experiments, we find that the best range of k_0 is from 20 to 40. Here, we set k_0 as 20.

The parameter n_{iter} is the iteration number. We integrate n_{iter} into the diffusion coefficient, as shown in (16). If n_{iter} is set to a large number, a small diffusion coefficient will be obtained. This strategy will overcome the problem inherent in the traditional AD model that tends to decrease the edge feature contrast as n_{iter} increases. Fig. 5 depicts the despeckled results of different n_{iter}. In the case of $n_{iter} = 8$, our filter has removed the speckle noise while preserving features properly. As the n_{iter} increases, features are all effectively protected to the same extent. To reduce the required time for despeckling, we set $n_{iter} = 8$.

The final optimal parameter configurations of the proposed PFDTV method are set as $\Delta t = 0.15, s = 15, k_0 = 20, n_{iter} = 8$. Both the NLLRF and PFDTV methods are employed to perform visual comparison on the same public dataset. Therefore, we set the parameters according to the original paper of NLLRF [20]. Regarding the rest of the filters, we adjust the parameters for each filter to obtain the best visual effect. The final optimal parameter configurations for each filter are set as: 1) Frost: $W = 5 \times 5$, 2) SRAD: $\Delta t = 0.1, n_{iter} = 120$, 3) OBNLM: $M = 3, \alpha = 6, h = 1$, 4) SBF: $W = 3 \times 3, n_{iter} = 15$, 5) ADLG: $\Delta \mathrm{t} = 0.15, n_{iter} = 80$, and 6) NLLRF: $\beta = 10, H = 10$. Then, the filters were applied to clinical ultrasound images with their own parameter configurations.

Fig. 6 and Fig. 7 depict the despeckled results of different filters in the first row and show the corresponding local zoomed-in results in the second row. Visually, our method achieves the best performances in feature preservation and noise removal. According to the streak shown by the red arrow in Fig. 6, the PFDTV method produces the clearest edges. NLLRF only preserves a part of the streak while SRAD reduces the contrast of the streak heavily. Other filters remove the streak after speckle reduction. Similarly, according to the nodules indicated by the red arrow in Fig. 7, the PFDTV method succeeds in enhancing the local contrast. SRAD, OBNLM and NLLRF reduce the contrast of the nodules heavily. Other filters remove the nodules after despeckling.

To more closely evaluate despeckled images of different filters, we adopted the method in [70] which evaluates all the features located in a single scan line through the ultrasound image. Fig. 8 shows the despeckled images of different filters and their corresponding intensity value profile at the same scan line (marked as white solid line across the image in Fig. 8(a)). The intensity profile of scan line shows that, Frost, SRAD, SBF and ADLG all fail to maintain the edge contrast, reducing the visual effect. OBNLM and NLLRF succeed in enhancing the high-contrast edges in regions of interest (ROI) shown by the purple window. For low-contrast edges indicated by the red windows, both the OBNLM and NLLRF methods fail to preserve the local contrast of edge. As shown by the ROI in red windows in Fig. 8(h), after edge enhancement using adaptive fractional-order α, there are slight differences of edge contrast between the despeckled image of the PFDTV method and the original ultrasound image. Compared with other filters, the PFDTV method achieves the best performance in preserving the edge contrast. More despeckled results are depicted in Fig. 9. Obviously, the PFDTV method removes speckle noise thoroughly while preserving features satisfactorily.

C. Application to ultrasound image segmentation

For validating the performance of our method, we apply each filter to breast ultrasound (BUS) image segmentation. BUS images are commonly used to differentiate between benign and malignant tumours, which can be characterized by their shapes or contours of segmented breast lesions [8]. We first despeckle ten breast ultrasound images with differ-

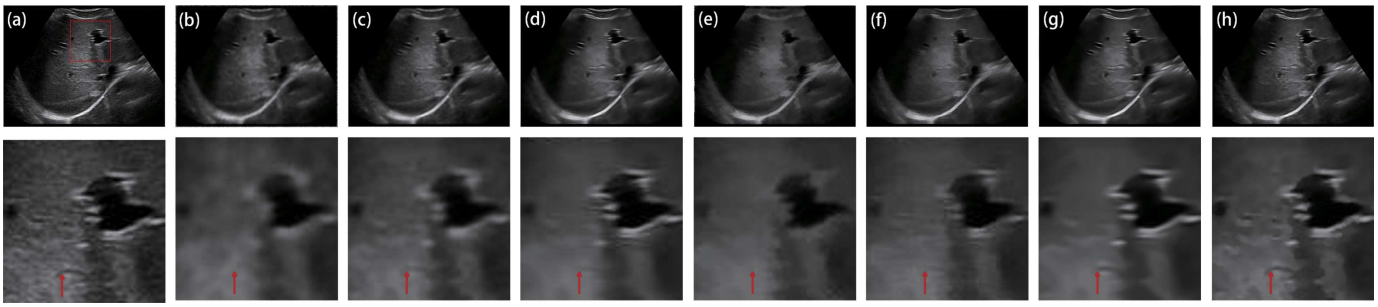

Fig. 6. Despeckled results of the ultrasound image of liver trauma and the corresponding zoomed details. (a) The original image; results by (b) Frost, (c) SRAD, (d) OBNLM, (e) SBF, (f) ADLG, (g) NLLRF, and (h) **PFDTV**.

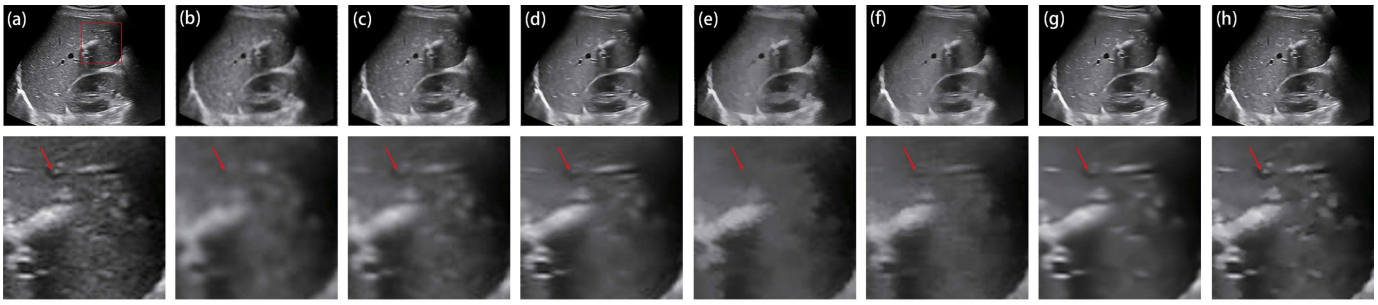

Fig. 7. Despeckled results of the ultrasound image of hepatitis and the corresponding zoomed details. (a) The original image; results by (b) Frost, (c) SRAD, (d) OBNLM, (e) SBF, (f) ADLG, (g) NLLRF, and (h) **PFDTV**.

ent lesions using different filters. A level-set method[71][4] is employed to segment the despeckled results. To validate the segmentation performance for all the ten images, we use the mean value of DSC metrics by averaging the metrics of ten segmentation results to evaluate each filter's despeckling effect on the segmentation performance. Specifically, we first set the range of related parameters of level-set method, then choose the optimal parameters that achieve the highest scores of the mean DSC for the ten BUS segmentation results. Fig. 10 displays the BUS segmentation[5]: the green curves are the segmentation results of different filters and the yellow curve is the ground truth delineated by an expert; after the speckle reduction, each filter improves the performance of the segmentation result compared with the original BUS image. Among these filters, the segmentation result based on the PFDTV filter is closest to the ground truth. The filtered lesions via other filters are very blurry so that the segmentation method [71] is not able to accurately delineate the lesions from these despeckled images.

We adopt four evaluation metrics [72], including the dice similarity coefficient (DSC) [40], Jaccard similarity (JS) [73], Hausdorff distance (HD) and Hausdorff mean (HM) [74] to measure the segmentation accuracy. As simple spatial overlap indices and producibility validation metrics, DSC and JS measure the overlapping rate between the obtained segmentation region and the ground truth. As effective distance metrics between two finite point sets, HD and HM compute the distance of the contours between the obtained segmentation region and the ground truth. Hence, a better segmentation result should have higher DSC and JS, as well as lower HD and HM. Table III and Table IV list the mean and median values of DSC, JS, HD and HM for different segmentation results on ten despeckled BUS images, respectively. Obviously, PFDTV achieves the largest DSC and JS values, as well as the smallest HD and HM values, which indicate that PFDTV achieves better segmentation performance compared with other filters.

The computation times for the OBNLM, NLLRF and PFDTV methods are measured and compared on a computer with an Intel(R) Core(TM) CPU at 2.71 GHz and with 8 GB RAM. The computation time of our method on Fig. 7(a) which is a 225×300 image is 86.54 seconds. OBNLM needs 2.85 seconds to obtain the denoised result while NLLRF needs 430.21 seconds. Although PFDTV is not the slowest but its most implementation is C++ code while OBNLM and NLLRF are implemented based on MATLAB, its computation is still inefficient since it needs many more pixels to calculate the fractional-order differential.

V. Discussion and Conclusion

Due to the outstanding performance, non-local filtering is becoming a widely accepted method in image restoration and denoising [75]. In ultrasound despeckling, several state-of-the-art non-local filters [6][9][10][18][20][76] were developed recently. Compared with other despeckling techniques, they all achieved the best performance of preserving features. To verify the performance of our method, two non-local filters including OBNLM and NLLRF were used for comparison. We find that non-local filters make some low-contrast features heavily blurred. This occurs because the patches around these features

[4]http://www.imagecomputing.org/~cmli/DRLSE/

[5]The segmentation results of different filters on the ten images are attached in the supplemental file.

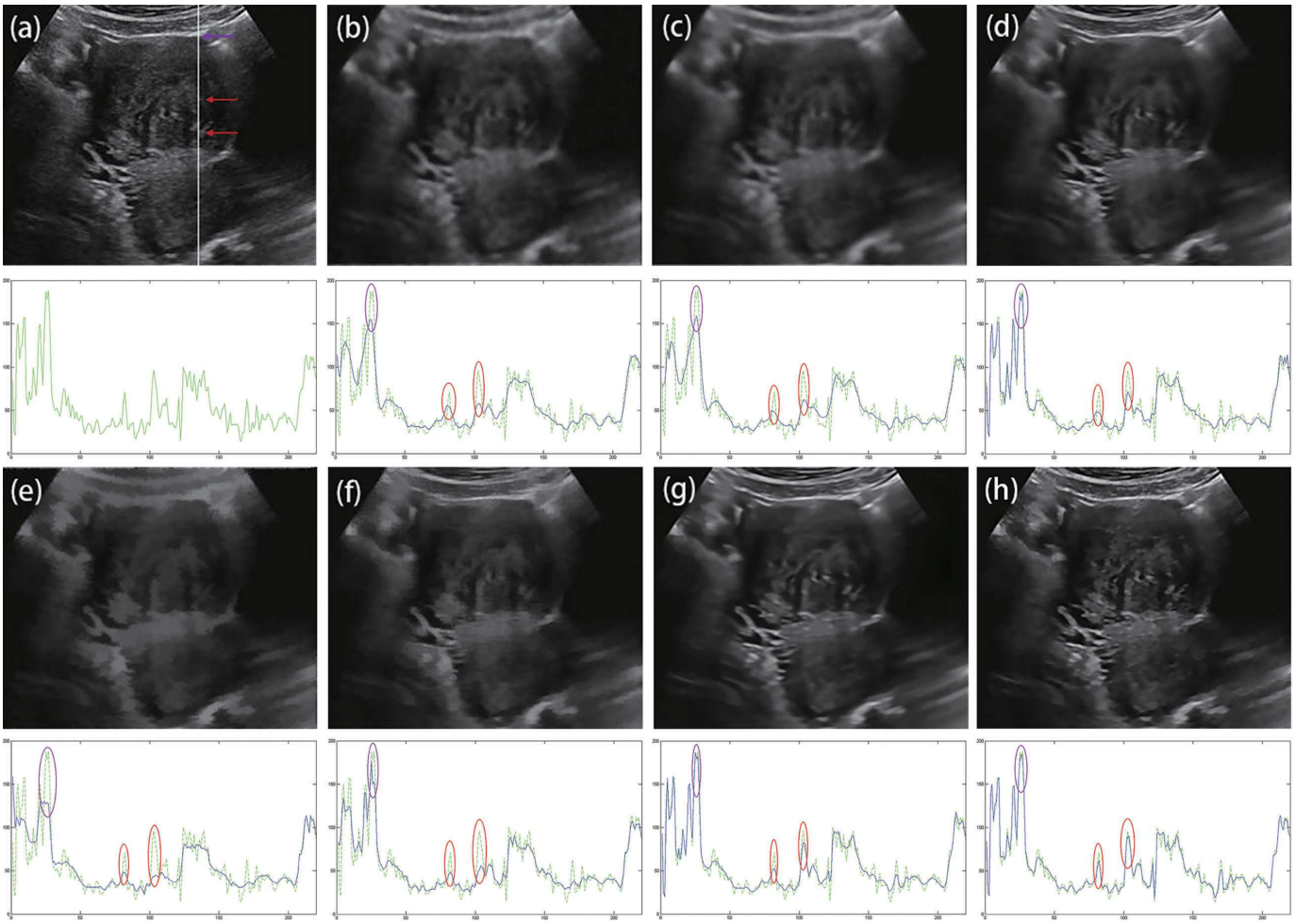

Fig. 8. Despeckled results of the ultrasound image of uterine fibroids and the corresponding intensity profiles at the same scan line in the white solid line in image (a). The intensity value profile of green line is for the original image while the blue line is for the filtered result of each filter. The purple windows indicate the ROIs for high-contrast edges, while the red windows for low-contrast edges. (a) The original image; the despeckled results by (b) Frost, (c) SRAD, (d) OBNLM, (e) SBF, (f) ADLG, (g) NLLRF, and (h) **PFDTV**.

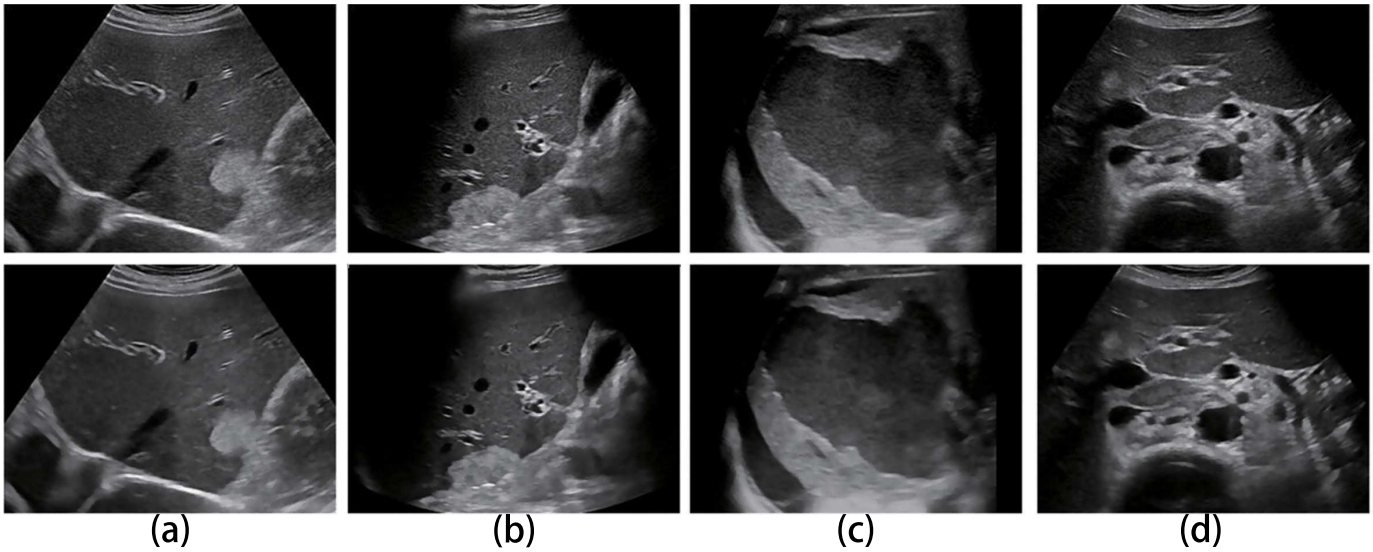

Fig. 9. More despeckled results of the proposed PFDTV method. First row: original ultrasound images; second row: the despeckled results. (a) ultrasound image of haemangiomas, ultrasound (b) image of haemangiomas, (c) ultrasound image of spleen trauma, and (d) ultrasound image of retroperitoneal lymph nodes and tumours image.

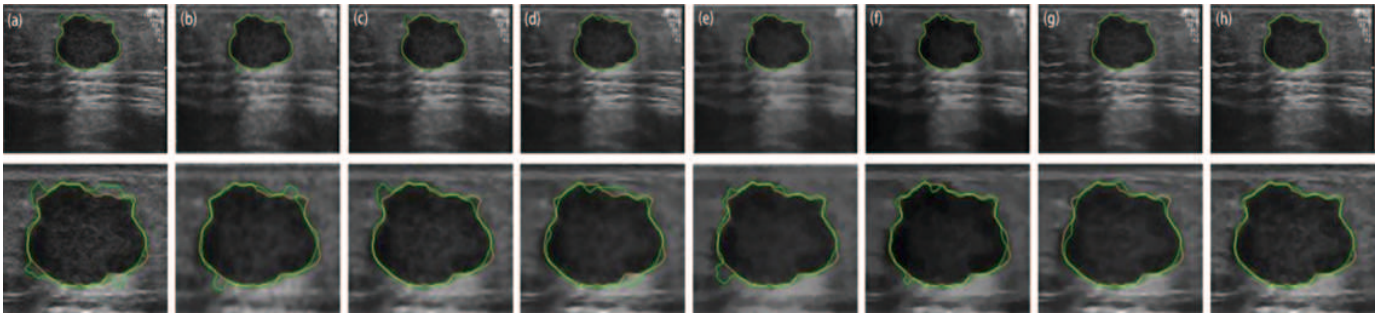

Fig. 10. The comparison of breast tumour segmentation on different despeckled results. Yellow colour: the ground truth delineated by an experienced clinician; Green colour: the segmentation results produced by . (a) The original ultrasound image and its segmentation result. Despeckled result and the corresponding segmentation results by (b) Frost, (c) SRAD, (d) OBNLM, (e) SBF, (f) ADLG, (g) NLLRF, and (h) **PFDTV**.

TABLE III
THE MEAN DSC, JS, HD AND HM VALUES FOR DIFFERENT SEGMENTATION RESULTS ON TEN BREAST ULTRASOUND IMAGES.

	DSC(%)	JS(%)	HD	HM
Input	91.87	85.02	16.9933	3.3599
Frost	93.62	88.02	9.8418	2.1265
SRAD	94.02	90.52	8.2271	1.5781
OBNLM	95.64	90.89	8.0608	1.6167
SBF	93.65	87.66	12.8664	2.0820
ADLG	94.92	90.37	9.0798	1.7034
NLLRF	95.39	91.21	7.2801	1.4977
PFDTV	**96.25**	**92.06**	**4.8441**	**1.2108**

TABLE IV
THE MEDIAN DSC, JS, HD AND HM VALUES FOR DIFFERENT SEGMENTATION RESULTS ON TEN BREAST ULTRASOUND IMAGES.

	DSC(%)	JS(%)	HD	HM
Input	91.63	84.56	16.8859	3.1183
Frost	93.12	87.12	8.9443	1.9195
SRAD	95.27	90.97	8.0868	1.5573
OBNLM	95.45	91.03	6.6623	1.6149
SBF	94.19	89.02	13.3033	1.9863
ADLG	94.99	90.49	8.0007	1.6920
NLLRF	95.5	91.39	7.0000	1.4623
PFDTV	**96.15**	**92.59**	**4.6926**	**1.3004**

are rather similar to the patch centred at speckle noise. After non-local filters remove noise by a weighted average of similar features, these low-contrast features will become indiscernible [39]. Compared with non-local filters, our method performs better in preserving features while removing noise thoroughly.

The most important feature of fractional models is non-locality. In our increasingly interconnected world, nonlocal interactions are becoming increasingly prominent to spur the studies on nonlocal modeling, analysis and computation. In computer vision and image processing, image denoising [35][77] can be understood as finding and averaging local and/or nonlocal similar patches for image reconstruction. The nonlocal similarity modeling that considers both geometric and photometric similarity [76][78] between the similar patches around reference and the selected pixels can be exploited to boost the performance of the feature-preserving ultrasound speckle filtering. In our previous work of texture-preserving nonlocal image denoising [2], the proposed ACVA method achieves excellent texture-preserving Gaussian and Poisson-Gaussian denoising performance both quantitatively and visually. Thus, an important future direction is to develop a nonlocal [79][80] version of the PFDTV method for enhancing the texture preservation in ultrasound despeckling.

Image denoising can also be considered as local and nonlocal regression problem [35][77][81] that reconstucts the origial signal from local and nonlocal noisy measurments. Most importantly, 3D ultrasound imaging [7][82] has benefitted a lot from deep learning methods, where deep encoder–decoder architectures serve as a general model for many regression problems and are widely used in computer vision and medical imaging. However, the large flexibility and capacity of deep learning architectures can make them overparameterized for removing the complex speckle noise from ultrasound image. Therefore, how to develop generative adversarial network and/or fractional-order deep network [83] to deal with the statistical characteristic of the signal-dependent speckle noise for improving computational efficiency and accuracy will be interesting research topics in future.

This paper uses the setting of fixed scale s to simplify our ultrasound despeckling computation without sacrificing significant despeckling performance when the fixed scale being integrated with adaptive fractional order during ultrasound despeckling. The solely setting of fixed scale [39] delivered a less satisfactory performance compared with updating optimal scale for each iteration during ultrasound despeckling. Future work will explore updating scheme with locally adaptive estimation of optimal scale that characterizes the intrinsic local salient structure [38][39] in ultrasound images.

In conclusion, we have proposed a phase asymmetry guided adaptive fractional-order TV framework combining FAD and FTV filters to achieve feature-preserving ultrasound despeckling. Synthetic and clinical ultrasound image experiments indicate that the proposed fractional-order TV filter outperforms other well-known ultrasound despeckling filters in both speckle reduction and feature preservation.

ACKNOWLEDEGMENT

The authors would like to thank all the cited authors for providing the source codes used in this work and the anonymous reviewers for their valuable comments on the manuscript.

REFERENCES

[1] Mishra D, Chaudhury S, Sarkar M, *et al.* Edge probability and pixel relativity-based speckle reducing anisotropic diffusion. IEEE Transactions on Image Processing, 2018, 27(2): 649-664.

[2] Zhao W, Liu Q, Lv Y, Qin B, Texture variation adaptive image denoising with nonlocal PCA, IEEE Transactions on Image Processing, 2019, 28(11): 5537-5551.

[3] Jeelani H, Liang H, Acton S T, *et al.* Content-Aware Enhancement of Images with Filamentous Structures. IEEE Transactions on Image Processing, 2019, in preprint.

[4] Zhao Y, Zhao Y, Zheng Y, *et al.* Automatic 2D/3D Vessel Enhancement in Multiple Modality Images Using a Weighted Symmetry Filter, IEEE Trans. Med. Imaging, 2018, 37(2):438-50.

[5] Joel T, Sivakumar R. An extensive review on Despeckling of medical ultrasound images using various transformation techniques. Applied Acoustics, 2018, 138: 18-27.

[6] Zhan Y, Ding M, Wu L, *et al.* Nonlocal means method using weight refining for despeckling of ultrasound images, Signal Processing, 2014, 103(C):201-213.

[7] Guo R, Lu G, Qin B, *et al.* Ultrasound imaging technologies for breast cancer detection and management: a review. Ultrasound in medicine & biology, 2018, 44(1): 37-70.

[8] Flores WG, de Albuquerque Pereira WC, Infantosi AFC. Breast Ultrasound Despeckling Using Anisotropic Diffusion Guided by Texture Descriptors, Ultrasound in Medicine & Biology, 2014, 40(11):2609-21.

[9] Song P, Trzasko JD, Manduca A, Huang R, Kadirvel R, Kallmes DF, and Chen S, Improved Super-Resolution Ultrasound Microvessel Imaging With Spatiotemporal Nonlocal Means Filtering and Bipartite Graph-Based Microbubble Tracking. IEEE transactions on ultrasonics, ferroelectrics, and frequency control, 2018, 65(2):149-167.

[10] Afsham N, Rasoulian A, Najafi M, Abolmaesumi P, and Rohling R, Nonlocal means filter-based speckle tracking. IEEE transactions on ultrasonics, ferroelectrics, and frequency control, 2015, 62(8):1501-1515.

[11] Wagner RF, Smith SW, Sandrik JM, *et al.* Statistics of Speckle in Ultrasound B-Scans, IEEE Trans. Son. Ultrason, 2005, 30(3):156-163.

[12] Shan X, Sun J, Guo Z. Multiplicative Noise Removal Based on the Smooth Diffusion Equation[J]. Journal of Mathematical Imaging and Vision, 2019: 1-17.

[13] Bao L, Song Y, Yang Q, *et al.* Tree Filtering: Efficient Structure-Preserving Smoothing With a Minimum Spanning Tree, IEEE Trans. Image Proc., 2014, 23(2):555-69.

[14] Frost VS, Stiles JA, Shanmugan KS, *et al.* A model for radar images and its application to adaptive digital filtering of multiplicative noise, IEEE Trans. Pattern Anal. Mach. Intell., 1982, 4(2):157-66.

[15] Zhang J, Lin G, Wu L, et al. Wavelet and fast bilateral filter based de-speckling method for medical ultrasound images. Biomedical Signal Processing and Control, 2015, 18: 1-10.

[16] Chen Q, Montesinos P, Sun Q S. Ramp preserving Perona–Malik model[J]. Signal Processing, 2010, 90(6): 1963-1975.

[17] Tay PC, Garson CD, Acton ST, *et al.* Ultrasound despeckling for contrast enhancement, IEEE Trans. Image Proc., 2010, 19(7):1847-60.

[18] Coupe P, Hellier P, Kervrann C, *et al.* Nonlocal means-based speckle filtering for ultrasound images, IEEE Trans. Image Proc., 2009, 18(10):2221-9.

[19] Zhou Y, Zang H, Xu S, *et al.* An iterative speckle filtering algorithm for ultrasound images based on bayesian nonlocal means filter model. Biomedical Signal Processing and Control, 2019, 48: 104-117.

[20] Zhu L, Fu CW, Brown MS, *et al.* A Non-local Low-Rank Framework for Ultrasound Speckle Reduction, IEEE Conference on Computer Vision and Pattern Recognition, 2017:493-501.

[21] Zhao W, Lv Y, Liu Q, Qin B, Detail-preserving image denoising via adaptive clustering and progressive PCA thresholding, IEEE Access, 2018, 6:6303-15.

[22] Perona P and Malik J, Scale-space and edge detection using anisotropic diffusion, IEEE Trans. Pattern Anal. Mach. Intell., 1990, 12(7):629–39.

[23] Yu Y, Acton ST. Speckle reducing anisotropic diffusion, IEEE Trans. Image Proc., 2002, 11(11):1260-70.

[24] Aja-Fernández S, Alberola-López C. On the estimation of the coefficient of variation for anisotropic diffusion speckle filtering, IEEE Trans. Image Proc., 2006, 15(9):2694.

[25] Krissian K, Westin CF, Kikinis R, *et al.* Oriented Speckle Reducing Anisotropic Diffusion, IEEE Trans. Image Proc., 2007, 16(5):1412-24.

[26] Zhou Z, Guo Z, Dong G, *et al.* A doubly degenerate diffusion model based on the gray level indicator for multiplicative noise removal. IEEE Trans. Image Proc., 2015, 24(1): 249-260.

[27] Jain S K, Ray R K. Non-linear diffusion models for despeckling of images: achievements and future challenges[J]. IETE Technical Review, 2019: 1-17.

[28] Bai J, Feng XC. Fractional-Order Anisotropic Diffusion for Image Denoising, IEEE Trans. Image Proc., 2007, 16(10):2492-502.

[29] Leal A S, Paiva H M. A new wavelet family for speckle noise reduction in medical ultrasound images[J]. Measurement, 2019, 140: 572-581.

[30] Gupta D, Anand R S, Tyagi B. Speckle filtering of ultrasound images using a modified non-linear diffusion model in non-subsampled shearlet domain[J]. IET Image Processing, 2015, 9(2): 107-117.

[31] Qiu Z, Yang L, Lu W. A New Feature-preserving Nonlinear Anisotropic Diffusion Method for Image Denoising, BMVC. 2011.

[32] Prasath V B S, Pelapur R, Seetharaman G, *et al.* Multiscale structure tensor for improved feature extraction and image regularization, IEEE Trans. Image Proc., 2019, 28(12): 6198-6210.

[33] Ofir N, Galun M, Alpert S, Brandt A, Nadler B, and Basri R. On Detection of Faint Edges in Noisy Images, IEEE Trans. Pattern Analysis and Machine Intelligence. doi: 10.1109/TPAMI.2019.2892134

[34] Cogranne R, Slysz R, Moreau L, *et al.* A new Edge Detector Based on Parametric Surface Model: Regression Surface Descriptor. arXiv preprint arXiv:1904.10235, 2019.

[35] Katkovnik V, Foi A, Egiazarian K, *et al.* From local kernel to nonlocal multiple-model image denoising. International journal of computer vision, 2010, 86(1): 1-32.

[36] Takeda H, Farsiu S, Milanfar P. Kernel regression for image processing and reconstruction[J]. IEEE Transactions on image processing, 2007, 16(2): 349-366.

[37] Qin B, Shen Z, Zhou Z, *et al.* Structure matching driven by joint-saliency-structure adaptive kernel regression. Applied Soft Computing, 2016, 46: 851-867.

[38] Qin B, Shen Z, Fu Z, *et al.* Joint-saliency structure adaptive kernel regression with adaptive-scale kernels for deformable registration of challenging images. IEEE Access, 2017, 6: 330-343.

[39] Zhu L, Wang W, Qin J, *et al.* Fast feature-preserving speckle reduction for ultrasound images via phase congruency, Signal Processing, 2017, 134:275-84.

[40] Belaid A, Boukerroui D, Maingourd Y, *et al.* Phase-based level set segmentation of ultrasound images, IEEE Trans. Infor. Tech. Biomed., 2011, 15(1):138-47.

[41] Morrone M C, Ross J, Burr D C, *et al.* Mach bands are phase dependent. Nature, 1986, 324(6094): 250-253.

[42] Morrone M C, Owens R A. Feature detection from local energy. Pattern recognition letters, 1987, 6(5): 303-313.

[43] Mulet-Parada M, Noble J A. 2D+T acoustic boundary detection in echocardiography[J]. Medical image analysis, 2000, 4(1): 21-30.

[44] Kovesi P. Image Features From Phase Congruency, Journal of Computer Vision Research, 1999, 1(3):1-26.

[45] Zhou G Q, Jiang W W, Lai K L, *et al.* Automatic Measurement of Spine Curvature on 3-D Ultrasound Volume Projection Image With Phase Features, IEEE Trans. Med. Imaging, 2017, 36(6):1250-62.

[46] Zhou Q, Gao J, Wang Z, *et al.* Adaptive Variable Time Fractional Anisotropic Diffusion Filtering for Seismic Data Noise Attenuation, IEEE Trans. Geoscience & Remote Sensing, 2016, 54(4):1905-17.

[47] Yu J, Tan L, Zhou S, *et al.* Image Denoising Algorithm Based on Entropy and Adaptive Fractional Order Calculus Operator, IEEE Access, 2017, 5:12275-12285.

[48] Zhou G Q, Jiang W W, Lai K L, *et al.* Automatic measurement of spine curvature on 3-D ultrasound volume projection image with phase features. IEEE transactions on medical imaging, 2017, 36(6): 1250-1262.

[49] Murray V, Rodríguez P, Pattichis M S. Multiscale AM-FM demodulation and image reconstruction methods with improved accuracy[J]. IEEE Trans. Image Proc., 2010, 19(5): 1138-1152.

[50] Havlicek J P, Tay P C, Bovik A C. AM-FM image models: Fundamental techniques and emerging trends[M]//Handbook of Image and Video Processing. Elsevier Inc., 2005: 377-395.

[51] Clausel M, Oberlin T, Perrier V. The monogenic synchrosqueezed wavelet transform: a tool for the decomposition/demodulation of AM–FM images. Applied and Computational Harmonic Analysis, 2015, 39(3): 450-486.

[52] Loizou C P, Murray V, Pattichis M S, *et al.* Multiscale amplitude-modulation frequency-modulation (AM–FM) texture analysis of ultrasound images of the intima and media layers of the carotid artery[J]. IEEE Trans. Information Technology in Biomedicine, 2010, 15(2): 178-188.
[53] Murray V, Pattichis M S, Barriga E S, *et al.* Recent multiscale AM-FM methods in emerging applications in medical imaging. EURASIP Journal on Advances in Signal Processing, 2012, 2012(1): 23.
[54] Felsberg M, Sommer G. The monogenic signal, IEEE Trans. Signal Proc., 2001, 49(12): 3136-3144.
[55] Boukerroui D, Noble JA, Brady M. On the Choice of Band-Pass Quadrature Filters, J. Math. Imaging Vis., 2004, 21(1-2):53-80.
[56] Love ER. Fractional Derivatives of Imaginary Order, Journal of the London Mathematical Society, 1971, s2-3(2):241-59.
[57] Oldham KB, Spanier. (1974) The fractional calculus: integrations and differentiations of arbitrary order, Academic Press, New York.
[58] Pu Y, Wang W, Zhou J, *et al.* Fractional differential approach to detecting textural features of digital image and its fractional differential filter implementation, Science in China, 2008, 51(9):1319-39.
[59] Ruding L, Osher S, and FatemiI E. Nonlinear Total Variation Based Noise Removal Algorithms. Phys. D, 1992, 60(1-4):259-68.
[60] Huang B, Mu Y, Pan Z, et al. Speckle noise removal convex method using higher-order curvature variation[J]. IEEE Access, 2019, 7: 79825-79838.
[61] Zhang J, Wei Z. Fractional Variational Model and Algorithm for Image Denoising, IEEE International Conference on Natural Computation, 2008:524-528.
[62] Riley KF, Hobson MP, Bence SJ, Mathematical Methods for Physics and Engineering: A Comprehensive Guide, 3rd Edition, Cambridge University Press, 2006.
[63] Wang D, Gao J. A new method for random noise attenuation in seismic data based on anisotropic fractional-gradient operators, Journal of Applied Geophysics, 2014, 110:135-143.
[64] Khvostikov A, Krylov A, Kamalov J, et al. Ultrasound despeckling by anisotropic diffusion and total variation methods for liver fibrosis diagnostics[J]. Signal Processing: Image Communication, 2017, 59: 3-11.
[65] Seshadrinathan K, Pappas TN, Safranek RJ, Chen J, Wang Z, Sheikh HR, & Bovik AC. Image quality assessment. In The essential guide to image processing (pp. 553-595), Academic Press, 2009.
[66] Huynh-Thu Q, Ghanbari M. Scope of validity of PSNR in image/video quality assessment. Electronics letters, 2008, 44(13): 800-801.
[67] Wang Z, Bovik AC, Sheikh HR, *et al.* Image quality assessment: from error visibility to structural similarity, IEEE Trans. Image Proc., 2004, 13(4):600.
[68] Zhang L, Zhang L, Mou X, *et al.* FSIM: A Feature Similarity Index for Image Quality Assessment, IEEE Trans. Image Proc., 2011, 20(8):2378-2386.
[69] Ramosllordén G, Vegassánchezferrero G, Martinfernandez M, *et al.* Anisotropic diffusion filter with memory based on speckle statistics for ultrasound images, IEEE Trans. Image Proc. 2015, 24(1):345-358.
[70] Aysal TC, Barner KE. Rayleigh-maximum-likelihood filtering for speckle reduction of ultrasound images, IEEE Trans. Med. Imaging, 2007, 26(5):712.
[71] C. Li, C. Xu, C. Gui, M.D. Fox, Distance regularized level set evolution and its application to image segmentation. IEEE Trans. Image Process, 2010, 19(12):3243–3254.
[72] Taha AA, Hanbury A. Metrics for evaluating 3D medical image segmentation: analysis, selection, and tool[J]. BMC medical imaging, 2015, 15(1): 29.
[73] Udupa J K, Imielinska C, Saha P K, *et al.* Methodology for evaluating image-segmentation algorithms[J]. Proceedings of SPIE - The International Society for Optical Engineering, 2002, 4684(4684):266-277.
[74] Cardoso F M, Matsumoto M M S, Furuie S S. Edge-Preserving Speckle Texture Removal by Interference-Based Speckle Filtering Followed by Anisotropic Diffusion[J]. Ultrasound in Medicine & Biology, 2012, 38(8):1414-1428.
[75] Shao L, Yan R, Li X, *et al.* From heuristic optimization to dictionary learning: a review and comprehensive comparison of image denoising algorithms, IEEE Trans. Cyber., 2014, 44(7):1001-1013.
[76] Santos CAN, Martins D LN, Mascarenhas NDA. Ultrasound Image Despeckling Using Stochastic Distance-Based BM3D, IEEE Trans. Image Proc., 2017, 26(6):2632-2643.
[77] Goyal B, Dogra A, Agrawal S, et al. Image Denoising Review: From classical to state-of-the-art approaches[J]. Information Fusion, 2020, 55:220-244.
[78] Santos C A N, Mascarenhas N D A. Geodesic distances in probabilistic spaces for patch-based ultrasound image processing[J]. IEEE Transactions on Image Processing, 2019, 28(1): 216-226.
[79] Yan Jin, Xiaoben Jiang, Wenyu Jiang, An Image Denoising Approach Based on Adaptive Nonlocal Total Variation, Journal of Visual Communication and Image Representation, 2019, https://doi.org/10.1016/j.jvcir.2019.102661.
[80] Pu Y F, Siarry P, Chatterjee A, et al. A fractional-order variational framework for retinex: fractional-order partial differential equation-based formulation for multi-scale nonlocal contrast enhancement with texture preserving[J]. IEEE Transactions on Image Processing, 2017, 27(3): 1214-1229.
[81] Zhu F, Qin B, Feng W, *et al.* Reducing Poisson noise and baseline drift in x-ray spectral images with bootstrap Poisson regression and robust nonparametric regression. Physics in Medicine & Biology, 2013, 58(6): 1739.
[82] van Sloun R J G, Cohen R, Eldar Y C. Deep learning in ultrasound imaging[J]. Proceedings of the IEEE, 2019, preprint, doi: 10.1109/JPROC.2019.2932116
[83] Jia X, Liu S, Feng X, et al. FOCNet: A Fractional Optimal Control Network for Image Denoising[C]//Proceedings of the IEEE Conference on Computer Vision and Pattern Recognition. 2019: 6054-6063.

Kunqiang Mei received the B.Sc. degree in Biomedical Engineering from Nanjing University of Aeronautics and Astronautics, Nanjing, and the M.Sc. degree in Biomedical Engineering from Shanghai Jiao Tong University, Shanghai, China, in 2016 and 2019, respectively. His current research interests include image processing, machine learning and computer vision.

Bin Hu received her MS and MD-PhD degrees from Tongji University and Shanghai Jiao Tong University, Shanghai, China, in 1997 and 2006, respectively. She is a member of the Superficial Organ and Peripheral Vascular Ultrasound Professional Committee of the China Ultrasound Medical Engineering Society and a member of the Ultrasound Branch of the China Association for the Advancement of Medical Sciences. Her current research interest is ultrasound diagnosis and interventional treatment of superficial organ diseases, especially breast diseases.

Baowei Fei is a professor in the Erik Jonsson School of Engineering and Computer Science, University of Texas at Dallas, USA. He received his MS and PhD degrees from Case Western Reserve University, Cleveland, Ohio. He is a director of the Quantitative Bioimaging Laboratory (https://fei-lab.org/) at Departments of Bioengineering and Computer Science in University of Texas at Dallas.

Binjie Qin (M'07) received his MS and PhD degrees from Nanjing University of Science and Technology, Nanjing, and Shanghai Jiao Tong University, Shanghai, China, in 1999 and 2002, respectively. He was a lecturer and then associate professor at School of Life Sciences and Biotechnology in Shanghai Jiao Tong University. From 2012 to 2013, He was a visiting professor at Department of Computer Science, University College London, U.K. He is currently an associate professor at School of Biomedical Engineering in Shanghai Jiao Tong University. His current research interests include biomedical imaging, image processing, machine learning, computer vision and biomedical instrumentation.